# *Pollution-derived $Br_2$ boosts oxidation power of the coastal atmosphere*

*Men Xia[1], Tao Wang[1]*, Zhe Wang[2], Yi Chen[2], Xiang Peng[4], Yunxi Huo[1], Weihao Wang[5], Qi Yuan[1], Yifan Jiang[1], Hai Guo[1], Chiho Lau[3], Kenneth Leung[3], Alfred Yu[3], and Shuncheng Lee[1]*

[1]Department of Civil and Environmental Engineering, The Hong Kong Polytechnic University, Hong Kong SAR, China

[2]Division of Environment and Sustainability, Hong Kong University of Science and Technology, Hong Kong SAR, China

[3]Air Science Group Environmental Protection Department, Hong Kong SAR, China

[4]China National Environmental Monitoring Centre, Beijing, China

[5]Hangzhou PuYu Technology Development Co Ltd, Hangzhou, Zhejiang, China

Correspondence: Tao Wang (tao.wang@polyu.edu.hk)

**KEYWORDS**

Molecular bromine, anthropogenic pollution, sea sprays, atmospheric oxidation, mercury, air quality

## ABSTRACT

The bromine atom (Br·) has been known to destroy ozone ($O_3$) and accelerate the deposition of toxic mercury (Hg). However, its abundance and sources outside the polar regions are not well known. Here we report significant levels of molecular bromine ($Br_2$)—a producer of Br·—observed at a coastal site in Hong Kong, with an average noontime mixing ratio of 5 ppt. Given the short lifetime of $Br_2$ (~1 min at noon), this finding reveals a large $Br_2$ daytime source. Based

on laboratory and field evidence, we show that the observed daytime $Br_2$ is generated by the photodissociation of particulate nitrate ($NO_3^-$), and that the reactive uptake of dinitrogen pentoxide ($N_2O_5$) on aerosols is an important nighttime source. Model-calculated Br· concentrations are comparable with the that of OH radical—the primary oxidant in the troposphere, accounting for 24% of the oxidation of isoprene, a 13% increase in net $O_3$ production, and a nearly 10-fold increase in the production rate of toxic $Hg^{II}$. Our findings reveal that reactive bromines play a larger role in the atmospheric chemistry and air quality of polluted coastal and maritime areas than previously thought. Our results also suggest that tightening control of emissions of two conventional pollutants ($NO_x$ and $SO_2$)—thereby decreasing the levels of nitrate and aerosol acidity—would alleviate the halogen radical production and its adverse impact on air quality.

**Table of Content art**

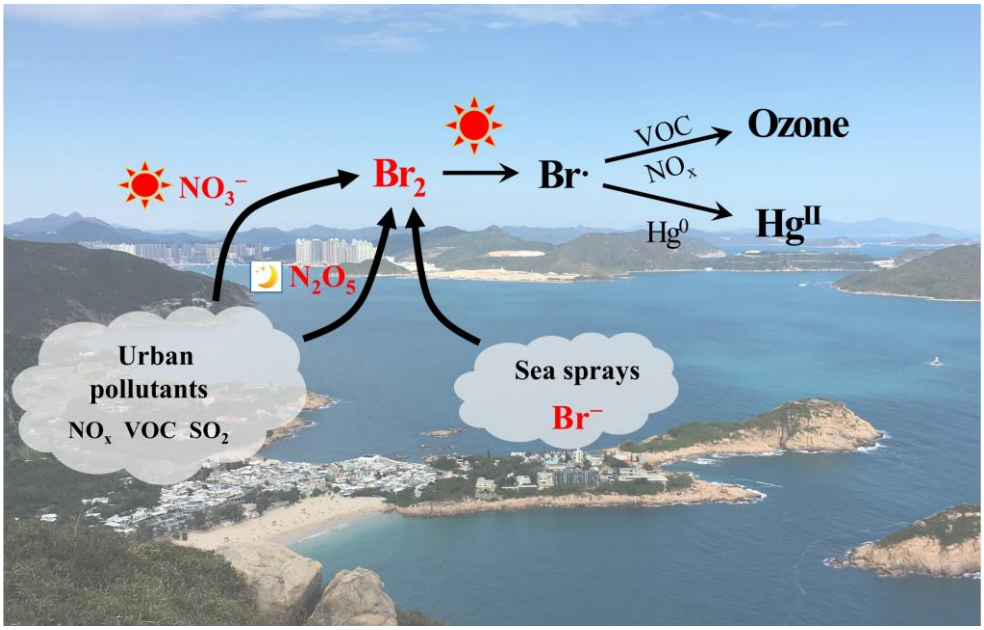


**SYNOPSIS**

$Br_2$ produced from pollution-sea spray interaction boosts atmospheric oxidation and affects coastal ecosystem.

## 1. Introduction

As a potent oxidizer, Br· has been recognized as the key species depleting $O_3$ in the Arctic and clean maritime atmospheres.[1-3] Br· also reacts with oxygenated volatile organic compounds (OVOCs) and alkenes to produce peroxy radicals and can produce $O_3$ and secondary aerosols in anthropogenically impacted regions.[4] Moreover, Br· oxidizes elemental mercury ($Hg^0$) to form $Hg^{II}$, which is neurotoxic to humans and other animals.[5, 6]

$Br_2$ is rapidly photolyzed by radiation, mainly in the wavelengths of 350–600 nm, to produce two Br atoms.[7] Previous studies have demonstrated that a substantial amount of $Br_2$ can be produced from the liberation of bromide ($Br^-$) via heterogeneous reactions on snow or ice; thus, $Br_2$ is an important source of Br· in the Arctic.[8] However, only a handful of studies have reported $Br_2$ concentrations in the extra-polar regions. Finley and Saltzman (2008)[9] reported an average $Br_2$ mixing ratio of 2.3 ppt at a polluted California coastal site in January 2006, with higher values in the nighttime. The source of $Br_2$ was not identified in that study. Breton et al. (2018)[10] reported aircraft measurements of $Br_2$ over the Western Pacific, reporting an average $Br_2$ mixing ratio of 0.5 ppt in the marine boundary layer (MBL). The observed $Br_2$ could not be reproduced by a widely used global chemical-transport model. Two other studies in continental areas have found that coal burning produces $Br_2$ and other reactive bromine gases, like BrCl.[11, 12] In addition to coal burning, the photolysis of particulate $NO_3^-$ was implicated as a possible daytime production pathway of reactive bromines.[12] However, the contribution of this pathway to ambient $Br_2$ was not

quantitatively determined. Clearly, our knowledge of the abundance and sources of $Br_2$ (and other Br·-producing reactive bromines) outside the polar regions is insufficient due to a lack of observations in diverse geographical areas. Moreover, state-of-the-art atmospheric models struggle to predict $Br_2$ (and other related bromines) due to our limited understanding of their emission and/or chemical processes—especially the photochemical production pathway.[4, 13, 14] These deficiencies have limited our capability to evaluate the impacts of halogen chemistry on troposphere chemistry, air quality, and climate.

In this work, we present recent field measurements of $Br_2$ and other reactive halogen species at a polluted coastal site in Hong Kong where very high levels of $Cl_2$ were reported in a previous study.[15] We found that $Br_2$ concentrations were the highest around noon, indicating the existence of a large photochemical source of $Br_2$. Based on the results from the field and subsequent laboratory experiments, we show that the ambient $Br_2$ production can be accounted for by the photolysis of $NO_3^-$ at the ambient levels of aerosol acidity and $Br^-$, and propose that the reactive uptake of $N_2O_5$ is an important nighttime source of $Br_2$. Calculations using a photochemical box model indicate that Br· concentrations are comparable with the conventional OH radical and substantially contribute to the oxidation of isoprene—one of the most important biogenic hydrocarbons, $O_3$ production, and substantial shortening of the lifetime of Hg. Our findings reveal the important roles of $Br_2$ in the atmospheric chemistry of the polluted maritime environments, as well as the quantitative relationship involved in $Br_2$ production, which will enable air quality models to better predict the abundance and atmospheric impacts of $Br_2$. We call for the consideration of reactive halogens in the development of air pollution regulations.

## 2. Materials and Methods

### 2.1. Field observations.

A field campaign was performed from October 6 to November 24, 2020, at a coastal ground site (22.21° N, 114.25° E) in a rural area (Cape D'Aguilar) at the southeast tip of Hong Kong Island, China (Supplementary Fig. S1). Details of the site are described in a previous study.[15] During the observation period, the intercepted air masses were mostly influenced by continental outflows and coastal air masses transporting regional anthropogenic pollution from urban Hong Kong, the adjacent PRD, and other regions of China (Supplementary Fig. S2). Local emission sources include ocean-going vessels traveling in nearby waters, natural vegetation consisting of deciduous and evergreen trees, and sparse country roads near the site. A small village with tens of residents is located ~2 km to the west of the observation site. The field study simultaneously measured reactive halogens, trace gases ($NO_x$, $NH_3$, CO, $SO_2$, $O_3$), aerosol mass concentration ($PM_{2.5}$ and $PM_{10}$), aerosol size distribution, aerosol ionic compositions (e.g., $Cl^-$ and $NO_3^-$), volatile organic compounds (VOCs), $NO_2$ photolysis frequency ($jNO_2$), and meteorological parameters (T and RH). Here we provide detailed descriptions on reactive halogen measurements and summarize other measurements in the supplementary information.

Reactive halogens were measured by an iodide-adduct time-of-flight chemical ionization mass spectrometer ($I^-$-Tof-CIMS, Aerodyne Research). The principles of $I^-$-Tof-CIMS have been described in detail by a previous study.[16] The reagent ions ($I^-$ and $I(H_2O)^-$) were produced by passing 1 Lpm of $CH_3I$-containing $N_2$ air through an inline ionizer ($^{210}Po$). We unambiguously identified the peaks of $Br_2$, BrCl, $Cl_2$, $ClNO_2$, HOCl, $C_2H_3O_2Br$, $C_2H_3O_2Cl$, $N_2O_5$, and HONO in the Tof-CIMS via high-resolution peak fitting and the verification of the halogen isotopic ratios,

according to the natural isotopic abundance of Cl and Br (Supplementary Fig. S3). The mean mass resolution was ~4800.

Background signals of the Tof-CIMS were determined by injecting zero air to Tof-CIMS every two to three days. The background concentrations during the study period were 0.25 ± 0.05 for $Br_2$ and 0.32 ± 0.06 ppt for BrCl, which were low and relatively stable compared with their respective ambient concentrations. To determine whether the change in ambient conditions affected the background signals, we evaluated the background signals for three days by passing ambient air through an alkaline glass wool scrubber to remove halogens for 4 min every 3 hours. The results confirmed there was little difference between the background signals determined using the two methods (< 20% or 0.1 ppt) (Supplementary Fig. S4). The detection limit was 0.22 ± 0.09 ppt for $Br_2$ and 0.14 ± 0.04 ppt for BrCl, determined as two times the standard deviation in their signals during the background testing (Supplementary Table S1).

The calibrations of $Br_2$, $Cl_2$, $N_2O_5$, $ClNO_2$, and $C_2H_3O_2Cl$ were performed onsite, and BrCl, HOCl, and HONO were calibrated in the laboratory right after the field study along with $Br_2$, $Cl_2$, $N_2O_5$, $ClNO_2$, and $C_2H_3O_2Cl$. $Br_2$, $Cl_2$, and $C_2H_3O_2Cl$ were calibrated once in the middle of the campaign using permeation tubes (KIN-TEC) with permeation rates of 150, 110, and 75 ng $min^{-1}$, respectively. The permeation rates of $Br_2$ and $Cl_2$ were verified by chemical titration using 2% KI solution followed by the measurement of light absorption at 351 nm using ultraviolet spectrophotometry.[12] BrCl was calibrated by placing the $Br_2$ and $Cl_2$ permeation tubes in the same oven where $Cl_2$ was in excess. HOCl was generated by passing ultrapure $N_2$ gas through NaOCl solution for HOCl calibration.[17] $N_2O_5$ was produced by mixing $NO_2$ and $O_3$ ($NO_2$ was in excess), and $ClNO_2$ was produced by passing $N_2O_5$ through a humidified NaCl slurry placed in a Teflon tube.[18] $N_2O_5$ and $ClNO_2$ were calibrated three times during the field study (on October 14 and

November 7 and 21), and their sensitivity was stable (difference < 10%). The sensitivity for $Br_2$ was 9.8 cps $ppt^{-1}$ in the presence of 1 million cps of reagent ions during the field study. To estimate the mixing ratio of $C_2H_3O_2Br$, we assumed the sensitivity ratio of $C_2H_3O_2Br$ to $Br_2$ was the same as that of $C_2H_3O_2Cl$ to $Cl_2$. The sensitivities of all calibrated species are summarized in Supplementary Table S1.

The Tof-CIMS was housed in a shelter, where the indoor air temperature was maintained at 25–28 °C by air conditioners. The sampling inlet was a 0.5-m long PFA tube (outer diameter: 0.50 inch; inner diameter: 0.44 inch) that penetrated the sidewall of the shelter, 1.5 m above ground level. A blower was used to draw the air sample through the tubing to reduce the residence time of the air in the inlet. A flow rate of 25 Lpm was adopted to achieve laminar flow in the sampling tube; the residence time was 0.1 s. The Tof-CIMS sampled 2 Lpm ambient air from a branch (a 0.25-inch PFA tube) of the sampling tube, and the remaining air mass was discarded. We investigated possible inlet artifacts by injecting known concentrations of $O_3$, $N_2O_5$, $ClNO_2$, and $Cl_2$ to the sample inlet onsite, and HOCl and HOBr in the laboratory, similar to our previous study.[12] We concluded that inlet artifacts had little influence on the data of $Br_2$, $N_2O_5$, $ClNO_2$, $Cl_2$, and BrCl (Supplementary Text S1).

## 2.2. E-AIM model and HYSPLIT backward trajectory.

The $[H^+]$ in the aqueous phase of ambient aerosols was calculated using the batch mode of the E-AIM model III online (http://www.aim.env.uea.ac.uk/aim/model3/model3a.php; last access: October 2021). Field measurement data of $NH_4^+$, $Na^+$, $SO_4^{2-}$, $NO_3^-$, and $Cl^-$ in $PM_{2.5}$ derived from aerosol filters (Supplementary Text S1) and the daily average of ammonia ($NH_3$) measured using

147 an $NH_3$ analyzer were used as the model input. The initial concentration of $H^+$ in the model was
148 set to balance the anion and cation charges. The E-AIM model configuration is as follows. Water
149 dissociation is always calculated, and both $H^+$(aq) and $OH^-$(aq) are regarded as variables in the
150 model. The partitioning of $HNO_3$, HCl, $NH_3$, and $H_2SO_4$ in gas and condensed phases is calculated.
151 The model is configured to allow for the formation of all possible solids in the system. Aerosol pH
152 was calculated as $-\log_{10}([H^+])$.

153 The Hybrid Single-Particle Lagrangian Integrated Trajectory (HYSPLIT) was obtained online
154 (https://www.ready.noaa.gov/hypub-bin/trajtype.pl?runtype=archive; last access: December
155 2021). The meteorology was selected as GDAS 1°. The source location was input as 22.209 N,
156 114.253 E. The trajectory was obtained every two hours during the observations period. The total
157 run time was 24 h. The level height was selected as 200 m.

158

159 2.3. Calculation of halogen yields from nocturnal $N_2O_5$ uptake

160 The halogen production yields from $N_2O_5$ uptake are defined analogously to those of $ClNO_2$.
161 The concept is similar to that in our previous work, in which we observed nighttime correlations
162 between $ClNO_2$ and $Cl_2$ and attributed $Cl_2$ production to $N_2O_5$ uptake.[19]

163 (E1) $$\varphi(Br_2) = \frac{d[Br_2]/dt}{k(N_2O_5)[N_2O_5]}$$

164 (E2) $$\varphi(BrCl) = \frac{d[BrCl]/dt}{k(N_2O_5)[N_2O_5]}$$

165 where $k(N_2O_5)$ is the first-order loss rate coefficient of $N_2O_5$ on aerosols.

(E3) $k(N_2O_5) = \frac{1}{4} \times c(N_2O_5) \times S_a \times \gamma(N_2O_5)$

where $c(N_2O_5)$ is the average molecular velocity of $N_2O_5$, and $S_a$ denotes the surface area density of aerosols. We derived $\gamma(N_2O_5)$, $\varphi(ClNO_2)$, $\varphi(Br_2)$, and $\varphi(BrCl)$ in selected cases. The selection criteria are the same to our previous work.[20] Briefly, we assumed stable air masses and a steady state of $N_2O_5$ (i.e., its chemical production equals its loss) during the night.[21] In addition, the products of $N_2O_5$ uptake should exhibit steady increasing trends and obvious correlations during the night. With these criteria, we found two applicable cases on the nights of November 21 (Fig. 2) and November 17 (Supplementary Fig. S5). The halogen yields derived here should be regarded as lower limits, as their loss processes (e.g., dry depositions) are not considered.

## 2.4. Laboratory studies.

We used a dynamic chamber to measure the $Br_2$ production rate by illuminating nitrate-halide solutions. The chamber and light source are described in detail in a previous study.[15] Briefly, the chamber is made of TEF Teflon, with the top side of the chamber sealed by a transparent Teflon film. The volume of the chamber is 1.875 L. A high-pressure xenon lamp was used to mimic solar radiations. A quartz petri dish containing 4 mL of solution was placed in the inner center of the bottom side to mimic the aerosol aqueous phase in the atmosphere. The equivalent surface area density of the aqueous phase in the chamber was $5.1 \times 10^5$ $um^2$ $cm^{-3}$ as calculated by dividing the illuminated area of the solution by the volume of the chamber. We added zero air (4 Lpm, 75% RH) in the chamber to deliver gas-phase products for real-time detection in the Tof-CIMS. In the laboratory experiment, the Tof-CIMS was calibrated using the same method as in the field study.

The background levels, sensitivities, and detection limits of halogen species and HONO are summarized in Supplementary Table S1.

The illuminated solutions were prepared by mixing sodium chloride (NaCl, Sigma-Aldrich brand, 99.999% purity, metal basis), sodium bromide (NaBr, Sigma-Aldrich, 99.999% purity, metal basis), ammonium nitrate ($NH_4NO_3$, Sigma-Aldrich, 99.9 % purity), and sulfuric acid ($H_2SO_4$, Sigma-Aldrich, 98% purity). The molarity of NaCl was fixed at 1 mol $L^{-1}$, and the molarity of NaBr was adjusted to achieve different $Cl^-$ to $Br^-$ ratio. The amount of $H_2SO_4$ was altered to adjust the pH (2–5). We also used the sea water sampled near the observation site to investigate the possible matrix effect of sea water components. In that case, only $NH_4NO_3$ and $H_2SO_4$ were added. We also dried the solutions using ultrapure $N_2$ air and illuminated the salts remaining in the petri dish in additional experiments. A summary of the illuminated samples is shown in Supplementary Table S2.

We used the method described in Peng et al. (2022)[15] to calculate the production rate of $Br_2$ ($P(Br_2)$) in the chamber, shown as follows.

(E4) $P(Br_2)$ = photochemical loss of $Br_2$ + advected loss of $Br_2$ from the chamber

$$= jBr_2 \times [Br_2] + Q/V \times [Br_2]$$

where $Q$ is the flow rate in the chamber (set to 4 Lpm), $V$ is the chamber volume (1.875 L), and $[Br_2]$ is the mixing ratio of $Br_2$ in the chamber outflow measured by the Tof-CIMS. $jBr_2$ is calculated using the irradiation spectrum of the lamp and the cross-sections and quantum yields of $Br_2$, as recommended by the International Union of Pure and Applied Chemistry (IUPAC) (https://iupac-aeris.ipsl.fr/index.html, last access: September 2021). The light absorption and

reflection by the transparent Teflon-film window or inner parts of the chamber were not considered in the $jBr_2$ calculation. A $Br_2$ photolysis experiment in the empty chamber was performed to determine the real $jBr_2$ in the chamber, which did not show significant bias from the theoretical value. The photolysis frequency of $Br_2$ ($jBr_2$, $8.09 \times 10^{-2}$ $s^{-1}$) in the chamber was ~3.5 times larger than the average daytime $jBr_2$ in our field study ($2.28 \times 10^{-2}$ $s^{-1}$ at 12:00 LT calculated by the Tropospheric Ultraviolet and Visible (TUV) radiation model and scaled by the field-observed $jNO_2$).

## 2.5. Box model.

The Framework for 0-D Atmospheric Modeling (F0AM version 4.0.2)[22] was used to investigate the impact of reactive bromine chemistry at the field site. We used Master Chemical Mechanism (MCM) v3.3.1[23] (http://mcm.york.ac.uk; last access: January 2022) as the chemical mechanism and incorporated the gas-phase bromine and chlorine chemistry compiled in our previous work.[12] The heterogeneous chemistry of reactive halogens was adopted and simplified as gas-phase reactions (Supplementary Text S2). Dilution and deposition were calculated as first-order loss reactions for each species. The diurnal averages of the field-observed reactive halogens and relevant species were constrained in the model every 5 min (Supplementary Table S3). We simulated a 24-h solar cycle for the campaign-averaged condition in three scenarios: (1) "with Br and Cl", where all reactive Br and Cl species ($Br_2$, BrCl, $Cl_2$, HOCl, and $ClNO_2$) were constrained by the observation data; (2) "with Cl", where only reactive Cl species ($Cl_2$, HOCl, and $ClNO_2$) were constrained; and (3) the base scenario ("without Br or Cl"), where no reactive halogens were constrained. The impact of Br· alone was determined by comparing scenarios 1 and 2, and the

combined impact of Br· and Cl· was obtained by comparing scenarios 1 and 3. For each scenario, the model was run three times to stabilize intermediates, and the results of the last run were adopted for further analysis.

To determine whether the current mechanisms (gas-phase reactions and heterogeneous uptake of HOBr, $BrONO_2$, and $O_3$) can explain the observed daytime $Br_2$, we initialized the observed concentrations of reactive halogens ($Br_2$, BrCl, $Cl_2$, HOCl, and $ClNO_2$) in another model run and predicted the evolvement of these reactive halogens in a daily cycle. We did not assign the initial concentrations of BrO, HOBr, $BrNO_2$, and $BrONO_2$ because we did not observe detectable levels of these species during the field study. Other observation data were constrained in the model. Details of the model configurations, input data, treatment of heterogeneous reactions, sensitivity tests, and calculations of $O_x$ production and loss are described in Supplementary Text S2.

## 3. Results and Discussion

### 3.1. Field measurements of reactive bromines

Ambient levels of reactive bromines were measured using a time-of-flight chemical ionization mass spectrometer (Tof-CIMS, Methods, section 1) at a rural coastal site in South China (Supplementary Fig. S1) during the autumn of 2020. It is the same site where very high levels of $Cl_2$ were observed in 2018[15]. During the observation period, continental outflows transported anthropogenic pollution from urban Hong Kong, the Pearl River Delta (PRD), and other parts of mainland China. The daily maximum mixing ratios of $O_3$ ranged from 30 to 100 ppb (1-hour averages) with an average of 65 ppb. The average $PM_{2.5}$ concentration was 17.6 ± 7.6 μg $m^{-3}$.

Other concurrently measured species are shown in Supplementary Fig. S6 and Table S4. These results indicate a moderate level of pollution during the study period. Biogenic emissions were also evident, and the average mixing ratio of isoprene was 0.17 ppb (Supplementary Table S3).

Significant levels of $Br_2$ were frequently observed, with a maximum mixing ratio of 11 ppt in 5-min averages (Fig. 1a). The $Br_2$ concentration showed an obvious daytime peak, with an average of 5 ppt, and a smaller nighttime peak was also evident (Fig. 1b). Given the short lifetime of $Br_2$ due to the high photolysis frequency ($2.28 \times 10^{-2}$ $s^{-1}$ at 12:00 local time [LT]), high daytime $Br_2$ concentrations indicate the presence of a substantial Br· source at the site. The daytime $Br_2$ levels were two to three times higher than those reported in coastal California[9], ten times higher than those observed in airborne observations over the MBL of the Western Pacific[24], and comparable or slightly lower than those measured in polar areas.[8] The $Br_2$ concentrations were higher in the continental outflows and much lower after the air masses had traveled over the ocean for 24 hours (Supplementary Fig. S2). As for the other reactive bromines, BrCl was detected and showed a similar diurnal pattern to $Br_2$ but at lower concentrations. BrO, HOBr, $BrNO_2$, and $BrONO_2$ were not detected because their signals were either below the instrument's limit of detection (for $BrNO_2$ and $BrONO_2$) or they suffered from interferences as reflected in the lack of correlation between their respective isotopic signals (for BrO and HOBr). High concentrations of reactive chlorine compounds, including $Cl_2$, HOCl, and $ClNO_2$, were observed (Supplementary Fig. S6).

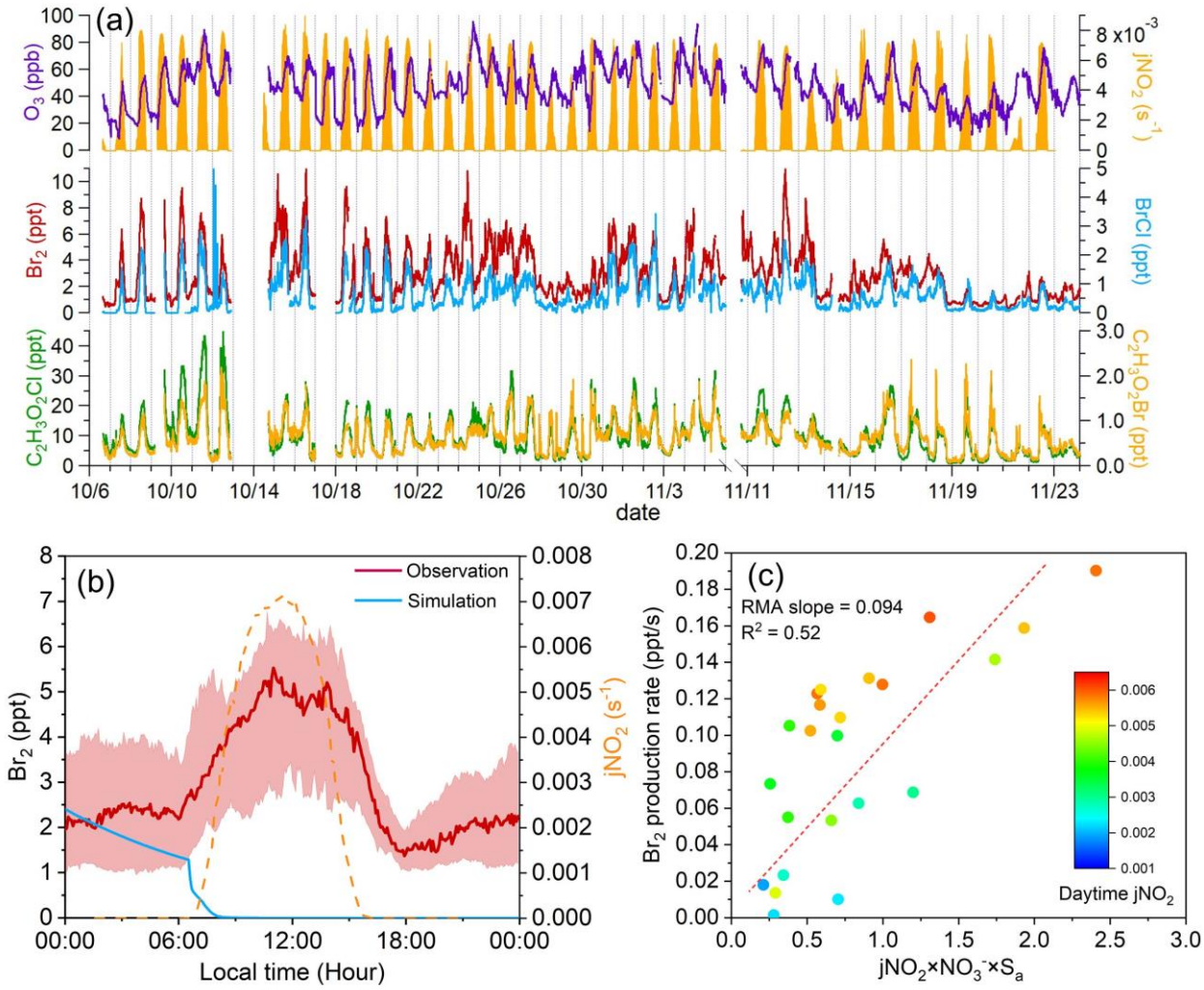


269

270 **Fig. 1** Field observations of reactive bromine at a coastal site (Cape D'Aguilar, Hong Kong). **(a)**
271 Time series of the mixing ratios of $Br_2$, BrCl, $C_2H_3O_2Cl$, $C_2H_3O_2Br$, $O_3$, and $NO_2$ photolysis
272 frequency ($jNO_2$) from October 6 to November 24, 2020. (Note: no halogen data were collected
273 on November 6-10 due to malfunction of the Tof-CIMS). **(b)** The average diurnal profile of the
274 observed $Br_2$ and the simulated $Br_2$. The orange dots show the $jNO_2$ values. **(c)** Relationship
275 between the $Br_2$ production rate ($P(Br_2)$, unit: ppt $s^{-1}$) and a proxy of $NO_3^-$ photolysis ($jNO_2 \times$
276 $NO_3^- \times S_a$). The color of the dots shows the $jNO_2$ ($s^{-1}$). The dashed red line shows a reduced major
277 axis (RMA) regression. The $P(Br_2)$, $jNO_2$, $NO_3^-$, and $S_a$ data are daily averages.

278

279 Besides reactive bromines, we also observed bromoacetic acid ($C_2H_3O_2Br$), a previously
280 unidentified brominated OVOC, in the ambient air. $C_2H_3O_2Br$ was moderately correlated with $Br_2$
281 ($R^2$ = 0.46, Supplementary Fig. S7), suggesting that $C_2H_3O_2Br$ could be a product of reactions
282 between Br· and ethene. Chloroacetic acid ($C_2H_3O_2Cl$) was also observed and correlated with $Cl_2$
283 ($R^2$ = 0.42, Fig. S7b). Priestley et al. (2018)[25] proposed that $C_2H_3O_2Cl$ could be an oxidation
284 product of Cl·. These results provide observational evidence for the Br and Cl oxidation of
285 hydrocarbons. We also searched for other possible markers of Br-containing volatile organic
286 compounds (VOC) but could not find detectable signals.

287

288 3.2. Pollution-derived $Br_2$ source

289 Considering the rapid photolysis of $Br_2$ that caused a photochemical lifetime of merely ~1 min
290 at noon in our study, a strong daytime source must exist to maintain and increase $Br_2$
291 concentrations in the daytime. The average production rate of $Br_2$ ($P(Br_2)$) at 12:00 LT was 0.11
292 ppt $s^{-1}$, assuming that $P(Br_2)$ equaled the photolysis rate of $Br_2$. Laboratory studies have reported
293 $Br_2$ productions from the uptake of $O_3$ and reactive bromines on acidic $Br^-$-containing surfaces,
294 including aerosols, chemical solutions, and snow/ice.[26] HOBr uptake on sea-salt aerosols[27] and
295 aqueous salt solutions (containing $Cl^-$ and $Br^-$)[28] produces $Br_2$ and BrCl, which supports the
296 autocatalytic release of inert $Br^-$ to reactive bromines (the "bromine explosion mechanism")
297 observed in Arctic regions.[8] Other $Br_2$ production pathways found in laboratory studies include
298 $BrONO_2$ uptake[29] and $O_3$ uptake[30] on NaBr solutions. However, we found that these mechanisms
299 cannot explain the observed $P(Br_2)$ at our site. We simulated the $Br_2$ levels by incorporating the

300 above heterogeneous reactions into a box model (Methods, section 5 and Supplementary Text S2),
301 initializing the reactive halogens according to our observations. The highest reported uptake
302 coefficient of HOBr (0.6) and unity yield of $Br_2$ following the halogen uptake reactions were
303 adopted to maximize $Br_2$ production in the model. The predicted $Br_2$ dropped to near-zero levels
304 in the morning (Fig. 1b). ~50% of Br· was lost via reactions with VOCs and OVOCs (Fig. 4a),
305 which reduced the Br· recycling efficiency and led to decreasing $Br_2$ levels during the daytime.
306 These results indicate that other source(s) of $Br_2$ are responsible for the daytime $Br_2$ observed at
307 our site.

308 We found a significant correlation between the daytime-averaged $P(Br_2)$ and the product of a
309 proxy of nitrate photolysis on aerosol surfaces ($jNO_2 \times NO_3^- \times S_a$) measured during the field study
310 ($R^2 = 0.52$, Fig. 1c). $P(Br_2)$ was substantially higher in the days with stronger solar radiation (i.e.,
311 higher $jNO_2$ in Fig. 1c). The correlation between the $P(Br_2)$ and $jNO_2 \times S_a$ was less significant ($R^2$
312 = 0.17). This result indicates that $NO_3^-$ plays a major role in the production of $Br_2$. The $Cl_2$
313 production rate ($P(Cl_2)$) was also correlated with $jNO_2 \times NO_3^- \times S_a$, consistent with our previous
314 findings at the same site.[15] Based on these field results, we propose that $NO_3^-$ photolysis produces
315 $Br_2$ via a mechanism similar to its $Cl_2$ production pathway[15], i.e., OH produced from $NO_3^-$
316 photolysis oxidizes $Br^-$ and forms $Br_2$ under acidic conditions (see reactions R1-R8). In the present
317 study, the aerosol pH was 2.66 ± 0.70 as estimated by the E-AIM model (Method, section 2),
318 indicating a moderately acidic condition.

319 (R1) $NO_3^-(aq) + hv\ (< 350\ nm) \rightarrow O^-(aq) + NO_2(g)$

320 (R2) $O^-(aq) + H^+(aq) \rightleftharpoons OH(aq)$

321 (R3) $OH(aq) + Br^-(aq) \rightleftharpoons HOBr^-(aq)$

(R4) $HOBr^-(aq) + H^+(aq) \rightleftharpoons HBrOH(aq)$

(R5) $HBrOH(aq) \rightleftharpoons Br(aq) + H_2O$

(R6) $Br(aq) + Br^-(aq) \rightarrow Br_2^-(aq) + H_2O$

(R7) $2Br_2^-(aq) \rightarrow Br_2(aq) + 2Br^-(aq)$

(R8) $Br_2(aq) \rightarrow Br_2(g)$

Nocturnal $Br_2$ production was also observed on some nights and related to the reactive uptake of $N_2O_5$ on $Br^-$-containing aerosols. The $Br_2$ produced via HOBr and $BrONO_2$ uptake should be negligible because their model-predicted levels dropped to zero at night (Supplementary Fig. S8). Figure 2a shows the nocturnal production of reactive halogens from $N_2O_5$ uptake on November 21, 2020 (Fig. 2a). The variation in $Br_2$ concentration was correlated with that of $ClNO_2$ ($R^2$ = 0.63, Fig. 2b), $Cl_2$ ($R^2$ = 0.85), BrCl ($R^2$ = 0.63), but not $O_3$ ($R^2$ = 0.11), HOCl ($R^2$ = 0.18), or other species. This result indicates that reactive halogens ($ClNO_2$, $Br_2$, $Cl_2$, and BrCl) were produced in parallel from $N_2O_5$ uptake. In our previous study,[19] we observed an obvious correlation between nighttime $Cl_2$ and $ClNO_2$ and concluded that they were parallel products from $N_2O_5$ uptake. Accordingly, we suggest that $Br_2$ was a co-product of $ClNO_2$ that originated from $N_2O_5$ uptake in this study. Analogous to the $Cl_2$ production by the $NO_2^+ + Cl^-$ reaction,[19] we suggest that $Br_2$ can also be produced via the oxidation of $Br^-$ by $NO_2^+$. $BrNO_2$ was not observed above the detection limit, suggesting efficient conversion from $BrNO_2$ to $Br_2$. This view is supported by previous laboratory experiments where simultaneous productions of $Br_2$ and $ClNO_2$ were observed after $N_2O_5$ uptake on halide-doped ice surfaces.[31] However, this $Br_2$ production pathway had not been observed in the field until the present study. Next, we calculated the kinetic parameters of nighttime $Br_2$ production, which are currently lacking in air quality models. $\gamma(N_2O_5)$ was determined as 0.055 by a steady-state method[21], and the $Br_2$ yield from $N_2O_5$ uptake was calculated

as $8.03 \times 10^{-4}$. The yields of other co-products were 0.84 for $ClNO_2$, $2.19 \times 10^{-3}$ for $Cl_2$, and $1.23 \times 10^{-4}$ for BrCl (Methods, section 3). A significant correlation between $Br_2$ and $ClNO_2$ was also observed on the nights of October 14, 25, and 31, and November 17 (Supplementary Fig. S5 and S9) but not every night, indicating the existence of other unknown nighttime sources. As nighttime $Br_2$ provides "seed bromine" that initiates the autocatalytic bromine cycle in the next morning,[32] future investigations of the nighttime production of $Br_2$ and other reactive bromines are merited.

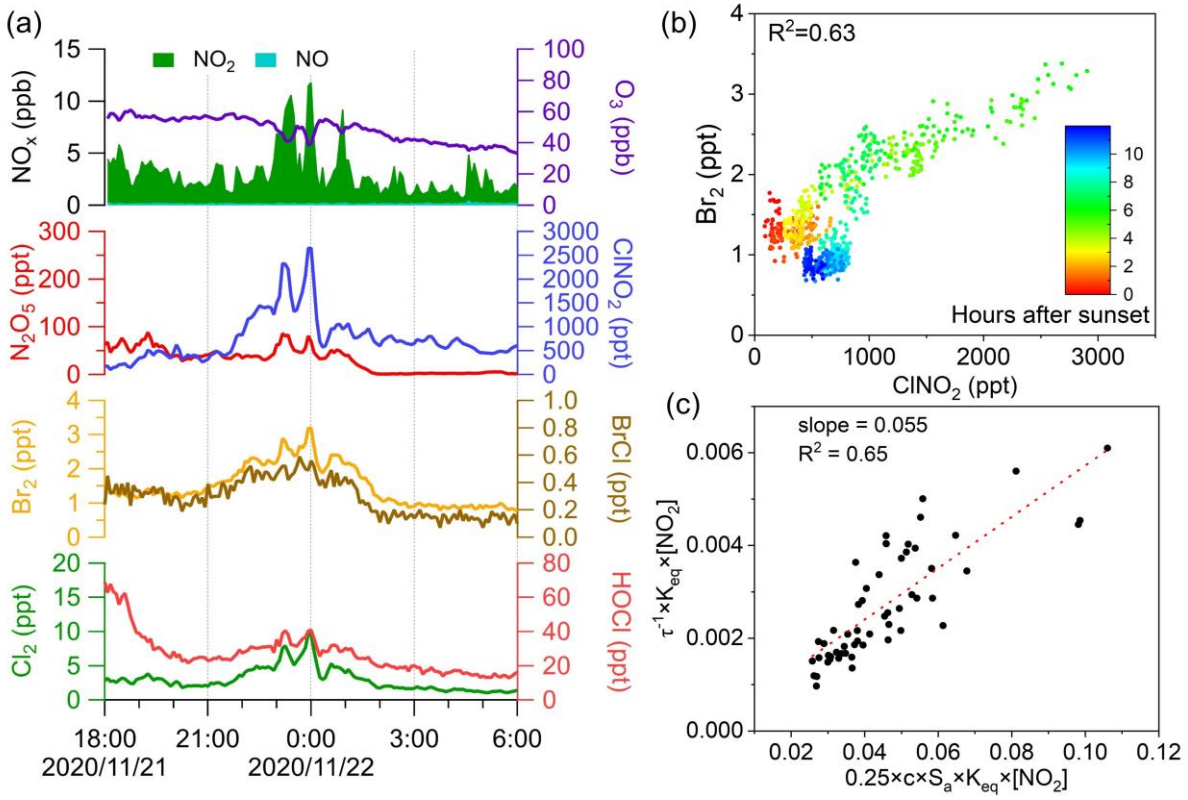


**Fig. 2.** A case study of the nocturnal production of reactive halogens from $N_2O_5$ uptake. **(a)** Field observations of reactive halogens and related species on the night of November 21, 2020. **(b)** Correlation between the mixing ratios of $Br_2$ and $ClNO_2$ during the night. The color bar shows the number of hours after sunset (18:00 LT). The $Br_2$ and $ClNO_2$ data are 5-min averages. **(c)** A steady-state analysis of $N_2O_5$ uptake during 19:00–23:55 on November 21 (Methods, section 3). The slope

of the red regression line represents $\gamma(N_2O_5)$. The 5-min averaged data were used to calculate $\tau^{-1} \times K_{eq} \times [NO_2]$ and $0.25 \times c \times S_a \times K_{eq} \times [NO_2]$.

### 3.3. Laboratory study of $Br_2$ production

We conducted a laboratory study to further investigate the role of $NO_3^-$ photolysis in $Br_2$ production by illuminating solutions that contain $NO_3^-$ and $Br^-$ in a dynamic chamber. We used solutions to perform experiments because a large proportion of ambient aerosols at our site should be in the aqueous phase under high RH conditions (75 ± 11%) during the field observation. Detailed information on the laboratory experiments is shown in Methods (section 4). Previous studies[33-35] have demonstrated that $Br_2$ can be produced by irradiating $NaNO_3$-NaBr solution, and that the acidity of the solution is important. In our study, we aimed to develop a quantitative relationship between $P(Br_2)$ and $NO_3^-$, $Br^-$, and acidity, which is indispensable in air quality models to predict the $Br_2$ production, and to demonstrate that this mechanism can explain the observed $P(Br_2)$ in the field. $Br_2$ and HONO were the dominant products in all experiments. BrCl was a minor product, and $Cl_2$ was not observed above the detection limit (see Fig. 3a for an example). This result is consistent with those of previous studies conducted under similar conditions.[33] To find out whether $Br_2$ could be produced by the photolysis of HONO in addition to nitrate, we conducted another experiment, which showed that $Br_2$ was not produced in the absence of nitrate (Text S3, Fig. S10). By using two optional filters to remove lights with wavelengths < 360 nm or allow lights with wavelengths in the 300–800 nm range to pass, we confirmed that $Br_2$ production mainly occurs at wavelengths lower than 360 nm.

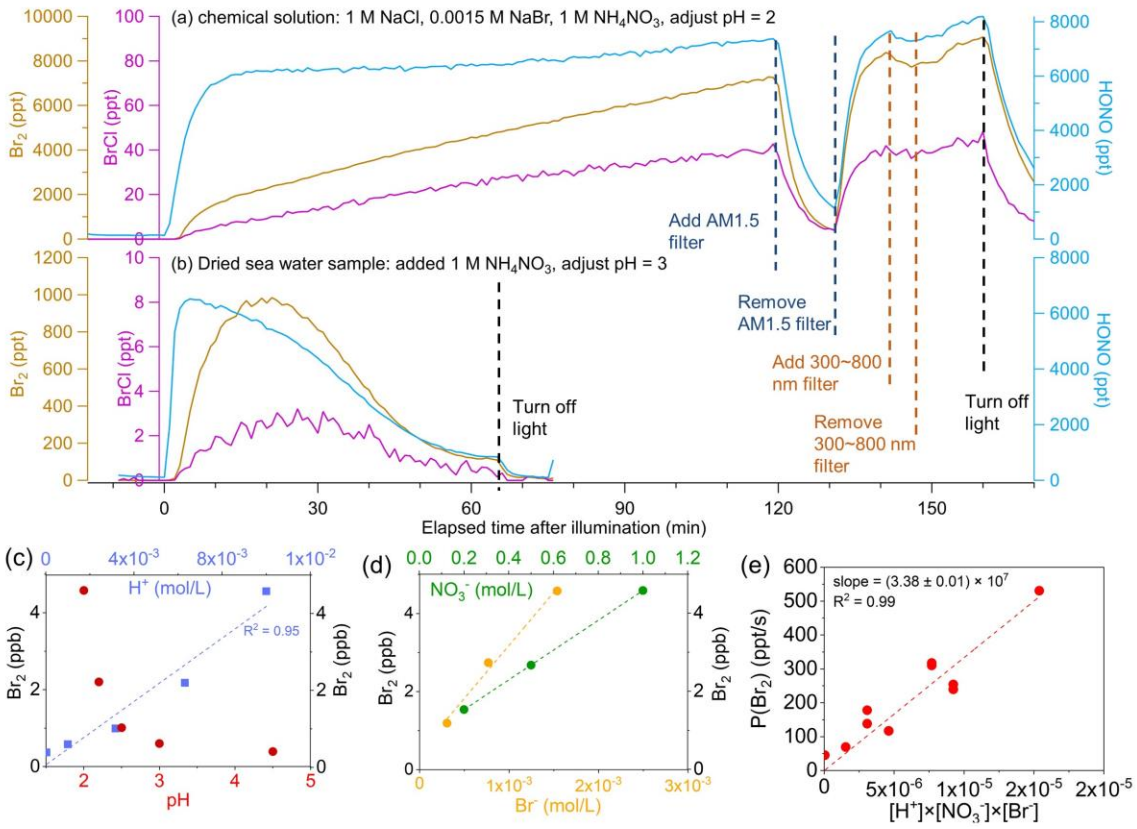


**Fig. 3.** Laboratory results of $Br_2$ production from the illumination of nitrate-halide solutions. **(a)** Production of $Br_2$, BrCl, and HONO as a function of the time after illuminating a NaBr-NaCl-$NH_4NO_3$ aqueous sample. The blue, orange, and black dashed lines show the operations of the optical filters and light sources, respectively. **(b)** Production of $Br_2$, BrCl, and HONO from the illumination of a dried sea-water sample with added $NH_4NO_3$ and $H_2SO_4$. **(c)** and **(d)** show the dependence of the $Br_2$ mixing ratio on $H^+$, pH, $NO_3^-$, and $Br^-$, after 1-h illumination. The pH was calculated as the negative logarithm of $[H^+]$ in the solution. **(e)** Relationship of $P(Br_2)$ and the product of $[H^+]$, $[NO_3^-]$, and $[Br^-]$ in the solution.

To mimic the ambient particles in polluted marine environments, we also illuminated authentic sea salts, which were produced by drying the seawater samples collected near the field site and

doped with $NH_4NO_3$ and $H_2SO_4$ (1 mol $L^{-1}$ $NO_3^-$, pH = 3) (Fig. 3b). Interestingly, the product ($Br_2$, HONO, and minor BrCl) concentrations showed peaks at or before 30 min of illumination and then gradually decreased to negligible levels, probably due to the depletion of surface-bonded $NO_3^-$ and $Br^-$. This phenomenon indicates that the surface availability and replenishment of $NO_3^-$ and $Br^-$ are important for $Br_2$ production and that the aerosol surface area density ($S_a$) is a critical parameter in $Br_2$ production.

$P(Br_2)$ was quantified in the solution experiments (without using seawater) as a function of $NO_3^-$, $Br^-$ and pH (or $H^+$) using equation (E4). The mixing ratio of $Br_2$ after a 60-min illumination was adopted in the calculation (Supplementary Text S4). The results show that the $Br_2$ production was positively correlated with $[H^+]$ (Fig. 3c), $[NO_3^-]$, and $[Br^-]$ (Fig. 3d) in the solution. Thus, the $P(Br_2)$ is correlated with the product of $[H^+]$, $[NO_3^-]$, and $[Br^-]$ ($R^2$ = 0.89, Fig. 3d). As $NO_3^-$ photolysis is an interfacial process on aerosol surfaces, we expect that $P(Br_2)$ would have a linear relationship with the $S_a$ of ambient aerosols. Thus, we propose that the ambient $P(Br_2)$ should be positively correlated with the product of $[H^+] \times [NO_3^-] \times [Br^-] \times jBr_2 \times S_a$ in the ambient air (equation E5).

(E5) $P(Br_2) = k \times [H^+] \times [NO_3^-] \times [Br^-] \times jBr_2 \times S_a$

where $k$ denotes an empirical pre-factor and has no explicit physical meaning, and $[H^+]$, $[NO_3^-]$, and $[Br^-]$ represent the aqueous-phase concentrations derived by the E-AIM model (Methods, section 2). The $jBr_2$ used here represents a measure of light intensity. In our laboratory experiments, the product of $k \times jBr_2 \times S_a$ corresponds to the slope of Fig. 3e ($3.38 \times 10^7$). Given that $jBr_2$ was $8.1 \times 10^{-2}$ and $S_a$ was $5.1 \times 10^5$ $um^2$ $cm^{-3}$ in the chamber, $k$ was determined to be 758.

We extrapolated the above laboratory result to estimate ambient $P(Br_2)$ from $PM_{2.5}$ during noontime (12:00 LT) at our site. The average concentrations of $H^+$, $NO_3^-$, and $Cl^-$ in the aqueous phase of aerosols during noontime were calculated as $2.2 \times 10^{-3}$, 2.7, and 2.6 mol $L^{-1}$ by the E-AIM model (Methods, section 2). The aqueous phase concentration of $Br^-$ in aerosols was estimated by assuming the same $[Cl^-]$ to $[Br^-]$ ratio in the aerosol liquid phase as that in the sea water (i.e., $[Cl^-]$:$[Br^-]$ = 650:1). The $S_a$ and $jBr_2$ at noon in our site were 328 $\mu m^2$ $cm^{-3}$ and $2.28 \times 10^{-2}$ $s^{-1}$, respectively. By applying these values to equation (E5), the average $P(Br_2)$ in ambient air was calculated to be 0.13 ppt $s^{-1}$ at noon, which is more than enough to explain the average field-observed $P(Br_2)$ of 0.11 ppt $s^{-1}$ (12:00 LT). Additional $Br_2$ production occurs on coarse-mode particles, which is not quantified in our study. The above analysis considered a simplified chemical system that contains only halide to consume OH. In the real atmosphere, organic components of aerosols are likely to compete with halide for aqueous-phase OH, reducing $Br_2$ production via $NO_3^-$ photolysis.[36, 37] Despite this uncertainty, we show that $NO_3^-$ photolysis is an important $Br_2$ production pathway at our site, and this process can be simulated by air quality models using the equation (E5) derived from our study.

### 3.4. Atmospheric impacts and implications

The impact of reactive bromines on atmospheric oxidation was evaluated by a chemical box model (Methods, section 5). The model was constrained by the observed reactive halogen concentrations and related data for campaign-averaged conditions. $Br_2$ photolysis was the largest primary source of Br·, directly contributing 63% Br· production (Fig. 4a) and serving as an indirect source by producing BrO that reacts with NO. BrCl was a minor source of Br· (2.6% direct

433 contribution) due to its lower concentrations and photolysis frequency. The predicted average
434 concentration of Br· was very high at noon ($3.5 \times 10^6$ molecules $cm^{-3}$), equal to 50% of the OH
435 concentration ($7\times 10^6$ molecules $cm^{-3}$) (Supplementary Fig. S11) and 15 times higher than the
436 previous Br· levels calculated at a coastal site in California.[9]

437

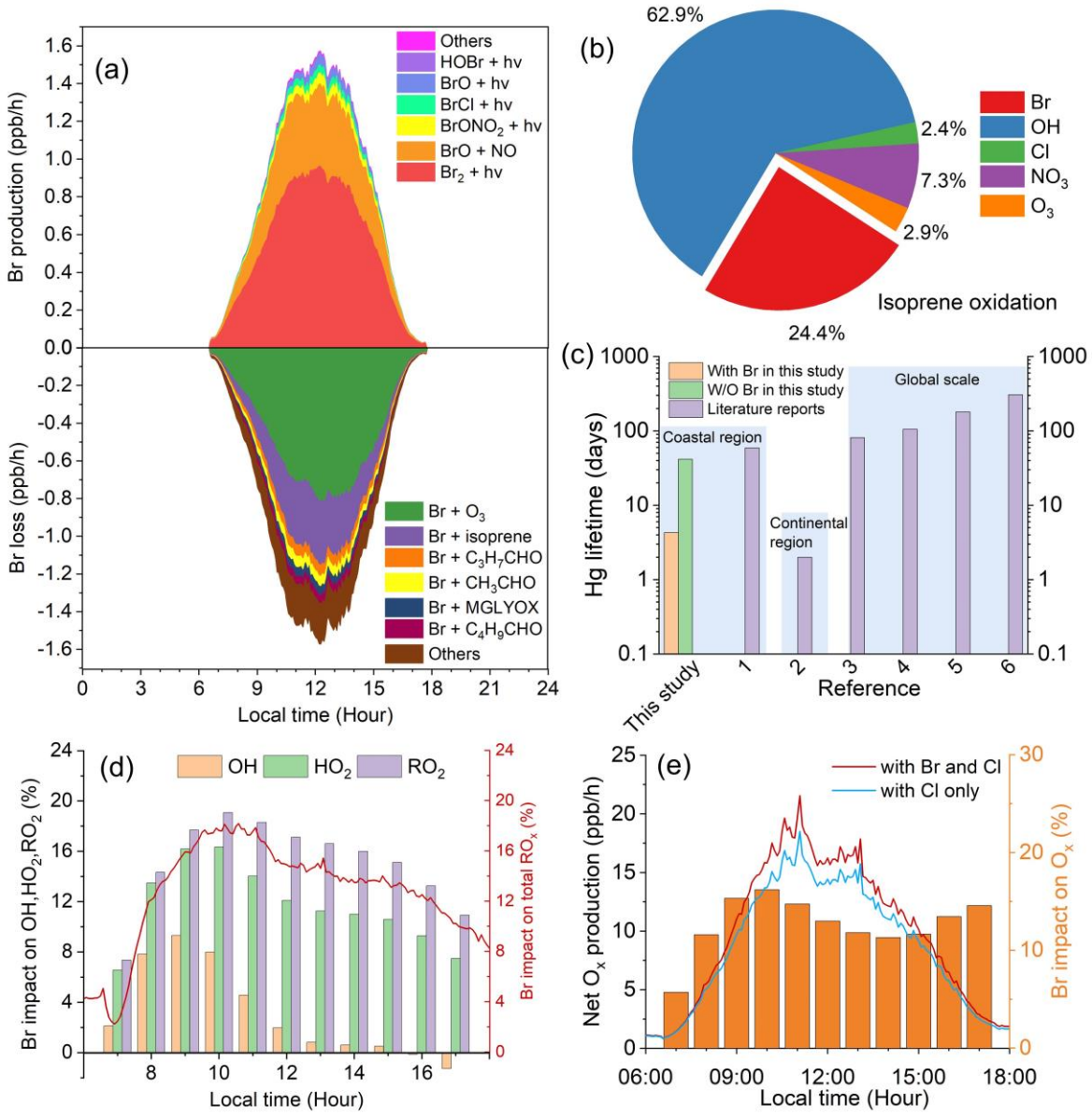


438

**Fig. 4.** Impacts of Br· on atmospheric oxidation for campaign-averaged conditions. **(a)** Diurnal variation of Br· production and loss rates. **(b)** Percentage contribution to isoprene oxidation by Br· and other oxidants. **(c)** A comparison of the Hg lifetime calculated in this study with those reported in the literature. References: 1. Finley and Saltzman, 2008[9]; 2. Peng et al. (2020)[12]; 3. Horowitz et al. (2017)[38]; 4. Saiz-Lopez et al. (2020)[39]; 5. Holmes et al. (2010)[40]; 6. Holmes et al. (2006)[41]. **(d)** Percentage change of $RO_x$ radicals due to Br·. The histogram shows the impacts of Br· on OH, $HO_2$, and $RO_2$, respectively, at different hours during the daytime. The red line shows the impact of Br· on total $RO_x$. **(e)** Impact of Br· on net $O_x$ ($O_3$ + $NO_2$) productions. Left axis: net $O_x$ production rate with Br (red line) and without Br (blue line) constrained. Right axis: the percentile impact of Br· on the net $O_x$ production shown by the orange histogram.

High levels of Br· have substantial impacts on VOC degradation, $RO_x$ (= OH + $HO_2$ + $RO_2$) radical levels, and $O_3$ formation. The daily integrated oxidation rates of VOCs were calculated for different oxidants (Br·, OH·, Cl·, $NO_3$·, and $O_3$) and VOC categories. Br· contributes 9.5% to the oxidation of alkenes, 6.6% for carbonyls, and 0.5% for aromatics, with a negligible effect on alkanes (Supplement Fig. S12). Particularly, Br· contributes to 19% of the oxidation of biogenic VOCs (BVOCs, including isoprene and terpenes), comparable to the contribution from $NO_3$· (20.3%). Br· is an especially important oxidant for the degradation of isoprene (contributing 24.4%, Fig. 4b), because Br· concentrations reach ~50% of OH levels, and Br· oxidizes isoprene almost as fast as OH does (Table S5).

The Br·-induced VOC oxidation increases the concentrations of OH, $HO_2$, and $RO_2$ radicals by 2.8%, 11.0%, and 14.2%, respectively, in the daytime (06:00–18:00 LT). Despite consuming $O_3$

via the reaction of Br· + $O_3$, Br· can promote $O_3$ production by enhancing $RO_x$ levels (Supplementary Fig. S13). The net effect is that Br· increases the net daytime $O_x$ ($O_3$ + $NO_2$) production by 13% (Fig. 4e). This result is consistent with that reported at a continental site in North China[12] but contrasts with the impacts observed in polar regions, where Br· largely consumes $O_3$.[8] When combined with Cl·, the halogen atoms (Br· and Cl·) caused even higher net $O_x$ productions (31%), revealing a substantial impact of halogen atoms on the $RO_x$ budget and $O_3$ at the study site.

We also calculated the lifetime of Hg by considering the two-step oxidation of $Hg^0$ to $Hg^{II}$ and the thermal decomposition of the $Hg^I$ intermediate (Supplementary Text S5). The model-calculated 24-h average concentrations of Br·, OH·, and Cl· and the observed $NO_2$ and $O_3$ levels were used for the calculations. The Hg lifetime was calculated to be 42 days without considering Br·, and only four days when Br· was considered. The calculated four-day lifetime is one to two orders of magnitude shorter than that estimated by global models[38-41] (Fig. 4c) and comparable with the short lifetime (~two days) at a continental site impacted by coal-burning emissions.[12] Our results are relevant to the current debate on the significant overestimate of Hg lifetime by global models and the cause for such discrepancy. A recent study proposed a new Hg oxidation mechanism besides the Br· oxidation pathway to reconcile the discrepancy between the observation-derived and modeled Hg lifetimes.[39] Our study suggests that the overestimate of Hg lifetime could also be due to the underestimation of $Br_2$ in the polluted MBL and subsequently Br· in current models. The shortening Hg lifetime by Br· would increase the deposition of land-emitted Hg near coastal oceans, adversely affecting marine life and the safety of seafood. As the largest marine fishery in the world, China harvested 15 million metric tons of aquatic products in 2016, mainly near the coasts of the Bohai Sea, East China Sea, and South China Sea.[42] The consumption

484 of coastal fish is the main pathway of human exposure to Hg, leading to high Hg content in humans
485 and related health problems in China.[43] Thus, atmospheric Hg deposition could aggravate the
486 threats of Hg to seafood safety and consumers' health.

487 In conclusion, this study reveals higher-than-expected $Br_2$ concentrations in a polluted coastal
488 area and considerable impacts on atmospheric chemistry and air quality, with implications for
489 seafood safety and marine ecosystems. Such impacts of reactive bromine may have been under-
490 recognized due to the lack of ambient reactive bromine measurements outside the polar regions,
491 which limits the awareness of their geographical presence and our ability to assess their impacts.
492 Our study demonstrates that a substantial amount of $Br_2$ can be produced by activating inert $Br^-$
493 via the photolysis of particulate $NO_3^-$ under acidic conditions. The co-existence of these conditions
494 is likely to occur in other places given ubiquitous presence of $NO_3^-$,[44] aerosol acidity,[45] and $Br^-$
495 from oceans and anthropogenic activities such as coal burning.[4, 12] Thus, $Br_2$ and other reactive
496 bromines could exist at sufficient concentrations to affect tropospheric oxidation. Therefore, we
497 call for more studies on the atmospheric abundance of reactive bromines and their sources and
498 impacts, especially in polluted regions.

499 The results of this study have important implications for air-pollution control policies. They
500 suggest that tightening control of emissions of two conventional pollutants, $NO_x$ and sulfur dioxide
501 ($SO_2$), would yield an air-quality co-benefit, namely, alleviating the halogen radical production and
502 its adverse impact on secondary pollutants from decreasing nitrate production and aerosol acidity.
503 $NO_x$ emission reduction is sometimes controversial in the formulation of air pollution regulations
504 because it can increase ozone pollution in urban areas due to the well-known $NO_x$ titration effect
505 for ozone. Our study indicates that reducing $NO_x$ emission – which slows the production of nitric
506 acid and particulate nitrate – would in turn decrease the promotion effect of reactive halogens on

ozone, which may offset some or all the ozone increase due to decrease in $NO_x$ emissions. Our findings, therefore, recommend strengthening the efforts to reduce emission of $NO_x$ (and $SO_2$). We also suggest controlling anthropogenic halogen emissions in future air pollution regulations.

## Supporting Information

Detailed information about the field observations in Hong Kong, dynamic chamber experiments, box model settings, and calculation processes of the Hg lifetime.


## Author Information

### Corresponding Author

**Tao Wang** − *Department of Civil and Environmental Engineering, The Hong Kong Polytechnic University, Hong Kong 999077, China*; Email: cetwang@polyu.edu.hk

### Authors

**Men Xia** − *Department of Civil and Environmental Engineering, The Hong Kong Polytechnic University, Hong Kong 999077, China*

**Zhe Wang** − *Division of Environment and Sustainability, Hong Kong University of Science and Technology, Hong Kong 999077, China*

**Yi Chen** − *Division of Environment and Sustainability, Hong Kong University of Science and Technology, Hong Kong 999077, China*

**Xiang Peng** − *China National Environmental Monitoring Centre, Beijing 100020, China*

**Yunxi Huo** − *Department of Civil and Environmental Engineering, The Hong Kong Polytechnic University, Hong Kong 999077, China*

**Weihao Wang** − *Hangzhou PuYu Technology Development Co Ltd, Hangzhou 311305, Zhejiang, China*

**Qi Yuan** − *Department of Civil and Environmental Engineering, The Hong Kong Polytechnic University, Hong Kong 999077, China*

**Yifan Jiang** − *Department of Civil and Environmental Engineering, The Hong Kong Polytechnic University, Hong Kong 999077, China*

**Hai Guo** − *Department of Civil and Environmental Engineering, The Hong Kong Polytechnic University, Hong Kong 999077, China*

**Chiho Lau** − *Air Science Group Environmental Protection Department, Hong Kong 999077, China*

**Kenneth Leung** − *Air Science Group Environmental Protection Department, Hong Kong 999077, China*

**Alfred Yu** − *Air Science Group Environmental Protection Department, Hong Kong 999077, China*

**Shuncheng Lee** − *Department of Civil and Environmental Engineering, The Hong Kong Polytechnic University, Hong Kong 999077, China*

## Author Contributions

T.W. designed the research. M.X., Y.C., and Z.W. performed Tof-CIMS measurements in the field. M.X. and Y.C. conducted measurements of particle size distributions, $NO_x$, $O_3$, and $jNO_2$. Q.Y. and SC.L. provided online OVOC data. H.G. provided aerosol chemical composition data. M.X. and Y.J. performed the laboratory work with the helpful discussions from X.P. and W.W.

M.X. performed the box model simulation with contributions from X.P. and W.W.. M.X. performed the E-AIM model simulation. Y.J. obtained the backward trajectory. M.X. and T.W. analyzed the field, laboratory, and modeling data. T.W. and M.X. wrote the paper. All authors contributed to paper revisions.

**Funding Sources**

This work is funded by the Hong Kong Research Grants Council (T24-504/17-N to T.W.).

**Notes**

The authors declare that they have no conflict of interests.

**ACKNOWLEDGMENT**

We thank the Hong Kong Environmental Protection Department for providing the field study site and data on trace gases, PM mass concentrations, VOCs, and OVOCs, the Hong Kong Observatory for providing the meteorological data, and the Hong Kong Polytechnic University Research Facility in Chemical and Environmental Analysis for providing the Tof-CIMS. We are grateful to Steven Poon for his help in logistics, and to Zhouxing Zou and Enyu Xiong for helpful discussions on the box model.

**REFERENCES**

1. Barrie, L. A.; Bottenheim, J. W.; Schnell, R. C.; Crutzen, P. J.; Rasmussen, R. A., Ozone destruction and photochemical reactions at polar sunrise in the lower Arctic atmosphere. *Nature* **1988,** *334* (6178), 138-141.

2. Solberg, S.; Schmidbauer, N.; Semb, A.; Stordal, F.; Hov, Ø., Boundary-layer ozone depletion as seen in the Norwegian Arctic in spring. *Journal of Atmospheric Chemistry* **1996,** *23* (3), 301-332.

3. Foster, K. L.; Plastridge, R. A.; Bottenheim, J. W.; Shepson, P. B.; Finlayson-Pitts, B. J.; Spicer, C. W., The role of $Br_2$ and BrCl in surface ozone destruction at polar sunrise. *Science* **2001,** *291* (5503), 471-474.

4. Li, Q.; Fu, X.; Peng, X.; Wang, W.; Badia, A.; Fernandez, R. P.; Cuevas, C. A.; Mu, Y.; Chen, J.; Jimenez, J. L.; Wang, T.; Saiz-Lopez, A., Halogens Enhance Haze Pollution in China. *Environmental Science & Technology* **2021,** *55* (20), 13625-13637.

5. Streets, D. G.; Horowitz, H. M.; Jacob, D. J.; Lu, Z.; Levin, L.; Ter Schure, A. F.; Sunderland, E. M., Total mercury released to the environment by human activities. *Environmental science & technology* **2017,** *51* (11), 5969-5977.

6. Obrist, D.; Kirk, J. L.; Zhang, L.; Sunderland, E. M.; Jiskra, M.; Selin, N. E., A review of global environmental mercury processes in response to human and natural perturbations: Changes of emissions, climate, and land use. *Ambio* **2018,** *47* (2), 116-140.

7. Sander, S. P.; Abbatt, J.; Barker, J.; Burkholder, J.; Friedl, R.; Golden, D.; Huie, R.; Kolb, C.; Kurylo, M.; Moortgat, G., Chemical kinetics and photochemical data for use in atmospheric studies, Evaluation No. 17. *JPL Publication* **2006,** (10-6).

8. Wang, S.; McNamara, S. M.; Moore, C. W.; Obrist, D.; Steffen, A.; Shepson, P. B.; Staebler, R. M.; Raso, A. R.; Pratt, K. A., Direct detection of atmospheric atomic bromine leading to mercury and ozone depletion. *Proceedings of the National Academy of Sciences* **2019**, 201900613.

9. Finley, B.; Saltzman, E., Observations of $Cl_2$, $Br_2$, and $I_2$ in coastal marine air. *Journal of Geophysical Research: Atmospheres* **2008,** *113* (D21).

10. Breton, M. L.; Hallquist, Å. M.; Pathak, R. K.; Simpson, D.; Wang, Y.; Johansson, J.; Zheng, J.; Yang, Y.; Shang, D.; Wang, H., Chlorine oxidation of VOCs at a semi-rural site in Beijing: significant chlorine liberation from $ClNO_2$ and subsequent gas-and particle-phase Cl–VOC production. *Atmospheric Chemistry and Physics* **2018,** *18* (17), 13013-13030.

11. Lee, B. H.; Lopez-Hilfiker, F. D.; Schroder, J. C.; Campuzano-Jost, P.; Jimenez, J. L.; McDuffie, E. E.; Fibiger, D. L.; Veres, P. R.; Brown, S. S.; Campos, T. L., Airborne observations of reactive inorganic chlorine and bromine species in the exhaust of coal-fired power plants. *Journal of Geophysical Research: Atmospheres* **2018,** *123* (19), 11,225-11,237.

12. Peng, X.; Wang, W.; Xia, M.; Chen, H.; Ravishankara, A. R.; Li, Q.; Saiz-Lopez, A.; Liu, P.; Zhang, F.; Zhang, C.; Xue, L.; Wang, X.; George, C.; Wang, J.; Mu, Y.; Chen, J.; Wang, T., An unexpected large continental source of reactive bromine and chlorine with significant impact on wintertime air quality. *National Science Review* **2020,** *8* (7), nwaa304.

609 13. Monks, P. S.; Archibald, A.; Colette, A.; Cooper, O.; Coyle, M.; Derwent, R.;
610 Fowler, D.; Granier, C.; Law, K. S.; Mills, G., Tropospheric ozone and its precursors from the
611 urban to the global scale from air quality to short-lived climate forcer. *Atmospheric Chemistry and*
612 *Physics* **2015,** *15* (15), 8889-8973.

613 14. Wang, X.; Jacob, D. J.; Downs, W.; Zhai, S.; Zhu, L.; Shah, V.; Holmes, C. D.;
614 Sherwen, T.; Alexander, B.; Evans, M. J., Global tropospheric halogen (Cl, Br, I) chemistry and
615 its impact on oxidants. *Atmospheric Chemistry and Physics* **2021**, *21* (18), 13973-13996.

616 15. Peng, X.; Wang, T.; Wang, W.; Ravishankara, A. R.; George, C.; Xia, M.; Cai, M.;
617 Li, Q.; Salvador, C. M.; Lau, C.; Lyu, X.; Poon, C. N.; Mellouki, A.; Mu, Y.;
618 Hallquist, M.; Saiz-Lopez, A.; Guo, H.; Herrmann, H.; Yu, C.; Dai, J.; Wang, Y.;
619 Wang, X.; Yu, A.; Leung, K.; Lee, S.; Chen, J., Photodissociation of particulate nitrate as a
620 source of daytime tropospheric $Cl_2$. *Nature Communications* **2022,** *13* (1), 939.

621 16. Lee, B. H.; Lopez-Hilfiker, F. D.; Mohr, C.; Kurtén, T.; Worsnop, D. R.; Thornton, J.
622 A., An Iodide-Adduct High-Resolution Time-of-Flight Chemical-Ionization Mass Spectrometer:
623 Application to Atmospheric Inorganic and Organic Compounds. *Environmental Science &*
624 *Technology* **2014,** *48* (11), 6309-6317.

625 17. Lawler, M. J.; Sander, R.; Carpenter, L. J.; Lee, J. D.; von Glasow, R.; Sommariva,
626 R.; Saltzman, E. S., HOCl and $Cl_2$ observations in marine air. *Atmospheric Chemistry and Physics*
627 **2011,** *11* (15), 7617-7628.

628 18. Xia, M.; Peng, X.; Wang, W.; Yu, C.; Wang, Z.; Tham, Y. J.; Chen, J.; Chen, H.;
629 Mu, Y.; Zhang, C., Winter $ClNO_2$ formation in the region of fresh anthropogenic emissions:
630 seasonal variability and insights into daytime peaks in northern China. *Atmospheric Chemistry and*
631 *Physics* **2021,** *21* (20), 15985-16000.

632 19. Xia, M.; Peng, X.; Wang, W.; Yu, C.; Sun, P.; Li, Y.; Liu, Y.; Xu, Z.; Wang,
633 Z.; Xu, Z.; Nie, W.; Ding, A.; Wang, T., Significant production of $ClNO_2$ and possible
634 source of $Cl_2$ from $N_2O_5$ uptake at a suburban site in eastern China. *Atmospheric Chemistry and*
635 *Physics* **2020,** *20* (10), 6147-6158.

636 20. Wang, Z.; Wang, W.; Tham, Y. J.; Li, Q.; Wang, H.; Wen, L.; Wang, X.; Wang,
637 T., Fast heterogeneous $N_2O_5$ uptake and $ClNO_2$ production in power plant and industrial plumes
638 observed in the nocturnal residual layer over the North China Plain. *Atmospheric Chemistry and*
639 *Physics* **2017,** *17* (20), 12361-12378.

21. Brown, S.; Ryerson, T.; Wollny, A.; Brock, C.; Peltier, R.; Sullivan, A.; Weber, R.; Dube, W.; Trainer, M.; Meagher, J., Variability in nocturnal nitrogen oxide processing and its role in regional air quality. *Science* **2006,** *311* (5757), 67-70.

22. Wolfe, G. M.; Marvin, M. R.; Roberts, S. J.; Travis, K. R.; Liao, J., The framework for 0-D atmospheric modeling (F0AM) v3.1. *Geoscientific Model Development* **2016,** *9* (9), 3309-3319.

23. Jenkin, M.; Young, J.; Rickard, A., The MCM v3.3.1 degradation scheme for isoprene. *Atmospheric Chemistry and Physics* **2015,** *15* (20), 11433.

24. Le Breton, M.; Bannan, T. J.; Shallcross, D. E.; Khan, M. A.; Evans, M. J.; Lee, J.; Lidster, R.; Andrews, S.; Carpenter, L. J.; Schmidt, J., Enhanced ozone loss by active inorganic bromine chemistry in the tropical troposphere. *Atmospheric Environment* **2017,** *155*, 21-28.

25. Priestley, M.; Breton, M. l.; Bannan, T. J.; Worrall, S. D.; Bacak, A.; Smedley, A. R.; Reyes-Villegas, E.; Mehra, A.; Allan, J.; Webb, A. R., Observations of organic and inorganic chlorinated compounds and their contribution to chlorine radical concentrations in an urban environment in northern Europe during the wintertime. *Atmospheric Chemistry and Physics* **2018,** *18* (18), 13481-13493.

26. Ammann, M.; Cox, R. A.; Crowley, J. N.; Jenkin, M. E.; Mellouki, A.; Rossi, M. J.; Troe, J.; Wallington, T. J., Evaluated kinetic and photochemical data for atmospheric chemistry: Volume VI – heterogeneous reactions with liquid substrates. *Atmospheric Chemistry and Physics* **2013,** *13* (16), 8045-8228.

27. Abbatt, J.; Waschewsky, G., Heterogeneous interactions of HOBr, $HNO_3$, $O_3$, and $NO_2$ with deliquescent NaCl aerosols at room temperature. *The Journal of Physical Chemistry A* **1998,** *102* (21), 3719-3725.

28. Fickert, S.; Adams, J. W.; Crowley, J. N., Activation of $Br_2$ and BrCl via uptake of HOBr onto aqueous salt solutions. *Journal of Geophysical Research: Atmospheres* **1999,** *104* (D19), 23719-23727.

29. Deiber, G.; George, C.; Calvé, S. L.; Schweitzer, F.; Mirabel, P., Uptake study of $ClONO_2$ and $BrONO_2$ by Halide containing droplets. *Atmospheric Chemistry and Physics* **2004,** *4* (5), 1291-1299.

30. Sakamoto, Y.; Goda, M.; Hirokawa, J., Kinetics Study of Heterogeneous Bromine Release from the Reaction between Gaseous Ozone and Aqueous Bromide Solution. *The Journal of Physical Chemistry A* **2018,** *122* (10), 2723-2731.

31. Lopez-Hilfiker, F.; Constantin, K.; Kercher, J.; Thornton, J. A., Temperature dependent halogen activation by $N_2O_5$ reactions on halide-doped ice surfaces. *Atmospheric Chemistry and Physics* **2012,** *12* (11), 5237-5247.

32. Simpson, W. R.; Brown, S. S.; Saiz-Lopez, A.; Thornton, J. A.; von Glasow, R., Tropospheric halogen chemistry: Sources, cycling, and impacts. *Chemical reviews* **2015,** *115* (10), 4035-4062.

33. Abbatt, J.; Oldridge, N.; Symington, A.; Chukalovskiy, V.; McWhinney, R. D.; Sjostedt, S.; Cox, R. A., Release of Gas-Phase Halogens by Photolytic Generation of OH in Frozen Halide−Nitrate Solutions: An Active Halogen Formation Mechanism? *The Journal of Physical Chemistry A* **2010,** *114* (23), 6527-6533.

34. George, I. J.; Anastasio, C., Release of gaseous bromine from the photolysis of nitrate and hydrogen peroxide in simulated sea-salt solutions. *Atmospheric Environment* **2007,** *41* (3), 543-553.

35. Richards, N. K.; Finlayson-Pitts, B. J., Production of gas phase $NO_2$ and halogens from the photochemical oxidation of aqueous mixtures of sea salt and nitrate ions at room temperature. *Environmental science & technology* **2012,** *46* (19), 10447-10454.

36. Herrmann, H.; Schaefer, T.; Tilgner, A.; Styler, S. A.; Weller, C.; Teich, M.; Otto, T., Tropospheric Aqueous-Phase Chemistry: Kinetics, Mechanisms, and Its Coupling to a Changing Gas Phase. *Chemical Reviews* **2015,** *115* (10), 4259-4334.

37. Anastasio, C.; Newberg, J. T., Sources and sinks of hydroxyl radical in sea‐salt particles. *Journal of Geophysical Research: Atmospheres* **2007,** *112* (D10).

38. Horowitz, H. M.; Jacob, D. J.; Zhang, Y.; Dibble, T. S.; Slemr, F.; Amos, H. M.; Schmidt, J. A.; Corbitt, E. S.; Marais, E. A.; Sunderland, E. M., A new mechanism for atmospheric mercury redox chemistry: implications for the global mercury budget. *Atmospheric Chemistry and Physics* **2017,** *17* (10), 6353-6371.

39. Saiz-Lopez, A.; Travnikov, O.; Sonke, J. E.; Thackray, C. P.; Jacob, D. J.; Carmona-García, J.; Francés-Monerris, A.; Roca-Sanjuán, D.; Acuña, A. U.; Dávalos, J. Z., Photochemistry of oxidized Hg(I) and Hg(II) species suggests missing mercury oxidation in the troposphere. *Proceedings of the National Academy of Sciences* **2020,** *117* (49), 30949-30956.

40. Holmes, C. D.; Jacob, D. J.; Corbitt, E. S.; Mao, J.; Yang, X.; Talbot, R.; Slemr, F., Global atmospheric model for mercury including oxidation by bromine atoms. *Atmospheric Chemistry and Physics* **2010,** *10* (24), 12037-12057.

41. Holmes, C. D.; Jacob, D. J.; Yang, X., Global lifetime of elemental mercury against oxidation by atomic bromine in the free troposphere. *Geophysical research letters* **2006,** *33* (20).

42. Zhang, W.; Liu, M.; Sadovy de Mitcheson, Y.; Cao, L.; Leadbitter, D.; Newton, R.; Little, D. C.; Li, S.; Yang, Y.; Chen, X., Fishing for feed in China: Facts, impacts and implications. *Fish and Fisheries* **2020,** *21* (1), 47-62.

43. Zhang, L.; Wong, M. H., Environmental mercury contamination in China: sources and impacts. *Environment international* **2007,** *33* (1), 108-121.

44. Bian, H.; Chin, M.; Hauglustaine, D. A.; Schulz, M.; Myhre, G.; Bauer, S. E.; Lund, M. T.; Karydis, V. A.; Kucsera, T. L.; Pan, X., Investigation of global particulate nitrate from the AeroCom phase III experiment. *Atmospheric Chemistry and Physics* **2017,** *17* (21), 12911-12940.

45. Pye, H. O. T.; Nenes, A.; Alexander, B.; Ault, A. P.; Barth, M. C.; Clegg, S. L.; Collett Jr, J. L.; Fahey, K. M.; Hennigan, C. J.; Herrmann, H.; Kanakidou, M.; Kelly, J. T.; Ku, I. T.; McNeill, V. F.; Riemer, N.; Schaefer, T.; Shi, G.; Tilgner, A.; Walker, J. T.; Wang, T.; Weber, R.; Xing, J.; Zaveri, R. A.; Zuend, A., The acidity of atmospheric particles and clouds. *Atmospheric Chemistry and Physics* **2020,** *20* (8), 4809-4888.